A transcriptional activator effector of *Ustilago maydis* regulates hyperplasia in maize during pathogen-induced tumor formation

Weiliang Zuo[1*], Jasper R. L. Depotter[1,4], Sara Christina Stolze[2], Hirofumi Nakagami[2,3], Gunther Doehlemann[1*]

1: Institute for Plant Sciences and Cluster of Excellence on Plant Sciences (CEPLAS), University of Cologne, Cologne 50674, Germany
2: Protein Mass Spectrometry, Max-Planck Institute for Plant Breeding Research, Carl-von-Linné Weg 10, 50829 Cologne, Germany
3: Basic Immune System of Plants, Max Planck Institute for Plant Breeding Research, Cologne 50829, Germany
4: Current address: Bioinformatics and Biostatistics, The Francis Crick Institute, 1 Midland Road, London, NW1 1AT, UK

***Correspondence to:** g.doehlemann@uni-koeln.de; wzuo@uni-koeln.de

Key words: *Ustilago maydis*, transcriptional activator, bundle sheath, hyperplasia tumor, leaf developmental regulators

Abstract

Ustilago maydis causes common smut in maize, which is characterized by tumor formation in aerial parts of the host. Tumors result from the *de novo* cell division of highly developed bundle sheath and subsequent cell enlargement. However, the molecular mechanisms underlying tumorigenesis are still largely unknown. Here, we characterize the *U. maydis* effector Sts2 (Small tumor on seedlings 2), which promotes the division of hyperplasia tumor cells. Upon infection, Sts2 is translocated into the maize cell nucleus, where it acts as a transcriptional activator, and the transactivation activity is crucial for its virulence function. Sts2 interacts with ZmNECAP1, a yet undescribed plant transcriptional activator, and it activates the expression of several leaf developmental regulators to potentiate tumor formation. Contrary, fusion of a suppressive SRDX-motif to Sts2 causes dominant negative inhibition of tumor formation, underpinning the central role of Sts2 for tumorigenesis. Our results not only disclose the virulence mechanism of a tumorigenic effector, but also reveal the essential role of leaf developmental regulators in pathogen-induced tumor formation.

Introduction

Plant pathogens secrete effectors to cross-talk with hosts for their benefits. To reshape the host transcriptome, some pathogens exploit effectors to directly manipulate host gene regulation in two main mechanisms. One is characterized by transcription activator-like (TAL) effectors, first described in the plant pathogenic *Xanthomonas sp*[1–3]. These effectors contain a nucleus localization signal, tandem repeat DNA binding domain and transcriptional activation domain, which can function independently as transcription factors to activate host gene expression. On the other hand, several effectors are not transcription factor themselves, but control host gene expression through interacting with host transcription factors[4], recruit the suppressors of transcription factors[5–8], or disrupt the assembly of transcription units[9,10], eventually leading to the inhibition or activation of host gene expression, respectively.

Ustilago maydis is a fungal pathogen which causes common smut in maize. It infects all the aerial maize organs, grows locally and produces massive amounts of teliospores[11,12]. To achieve this, *U. maydis* manipulates plant cell proliferation and thereby creates additional space in the form of tumors to reside in. On maize seedling leaves, tumors consist of hyperplasia tumor cells from the *de novo* division of highly differentiated bundle sheath tissue, some of such hyperplasia cells together with mesophyll enlarged to become hypertrophy tumor cells[13]. The host mechanisms of tumor formation and the causative effectors are still unknown. Until

now, the functionally characterized effectors in *U. maydis* are mainly involved in immunity inhibition[14–17] or host metabolism manipulation[18,19]. See1 is the only effector identified that is directly involved in tumorigenesis by re-activating DNA synthesis[20]; deletion of See1 causes the inhibition of *U. maydis* induced hyperplasia cell division[13]. Different tumor cells have a very different physiology and transcriptome in between, and compared to the sourced host cells[13,21]. One therefore can hypothesize that *U. maydis* possesses effectors to directly, or indirectly manipulate the host transcriptome. In line with this, several effectors of *U. maydis* have been identified to target Topless transcription co-repressors to modulate hormonal signaling and expression of immune genes during infection[6–8]. However, little is known about how effectors modulate the host transcriptome to induce tumors. A detailed *U. maydis* transcriptome analysis revealed the temporal regulation of effector genes throughout all steps of infection[22], and laser-captured microdissection of different tumor cells coupled with RNA-seq showed spatial, cell type specific regulation of effectors[13]. The cross-species analysis between *U. maydis* and *Sporisorium reilianum*, the closest smut relative which also infects maize but does not cause tumors, disclosed the differential regulation of effector orthologs that contribute to the distinct pathogenic development in the two species. A CRISPR-Cas9 mediated effector ortholog knock-in experiment discovered a functional diversification of an effector orthogroup UMAG_05318 - sr10075/ sr10079 during speciation[23].

In this study, we functionally characterized the effector Sts2 (UMAG_05318, Small tumor on seedlings 2). A *U. maydis* knockout strain for Sts2 (CR-Sts2) initiates tumor formation, but the tumors fail to expand due to reduced cell division of the bundle sheath. We discovered that Sts2 is a transcriptional activator, being translocated into host cell nucleus. It interacts with ZmNECAP1, a yet unknown plant transcriptional activator, to activate the expression of leaf developmental regulators. Sts2 transcriptional activation is crucial to maintain the meristem like cell divisions which lead to hyperplasic tumor cells. Our findings disclose a tumorigenic mechanism where a *U. maydis* small effector functions as a transcriptional activator in the host nucleus to rewrite the host developmental process by hijacking the key leaf developmental regulators.

Results

Sts2 regulates hyperplasia tumor cell induction by *U. maydis*

We generated an open reading frame shift knockout of *UMAG_05318* using CRISPR-Cas9 mutagenesis. The resulting mutant showed similarly reduced virulence **(Supplementary Fig.**

67 **1a)** as it was described previously for a deletion strain[24] **(Fig. 1a)**. Distinct from the typical
68 bulged tumors caused by *U. maydis* SG200, tumors induced by the UMAG_05318 knockout
69 mutant failed to expand in size **(Fig. 1a)**. Therefore, we named UMAG_05318 as Sts2 (Small
70 tumor on seedlings 2). Expression of *Sts2* starts from 1 dpi (days post infection), and peaks
71 between 2-4 dpi, when the tumor induction is initiated **(Supplementary Fig. 1b)**[22]. Wheatgerm
72 agglutinin-Alexa Fluor 488 (WGA-AF488) and propidium iodide co-staining showed no
73 obvious colonization defect in the CR-Sts2 mutant compared to SG200 at 2 dpi **(Fig. 1b)**. We
74 also monitored the growth of the mutant by relative fungal biomass quantification to 6 dpi **(Fig.
75 1c)**, the timepoint when leaf tumors get visible. Here, we did not detect a growth difference
76 between CR-Sts2 and SG200, suggesting that the defect of tumor formation is not caused by a
77 compromised biotrophic growth of the mutant, i.e. that Sts2 is probably not an inhibitor of host
78 immunity.
79 To further investigate how tumor formation is affected in the CR-Sts2 mutant, we
80 embedded 12 dpi leaves for transverse sectioning. In SG200 infected samples, clusters of small
81 hyperplasia tumor cells from *de novo* division of bundle sheath cells can be observed. These
82 were surrounded by 5-6 layers of supernumerary hypertrophic cells from enlarged divided cells
83 and mesophyll **(Fig. 1d, Supplementary Fig. 1b**), which is in accordance to our previous
84 observation[13]. Contrary, in CR-Sts2 infected plants, the *de novo* division was restricted, which
85 resulted in depletion of hyperplasia cells, as well as reduced layers of hypertrophic cells **(Fig.
86 1d, Supplementary Fig. 1b)**. In brief, knock-out of Sts2 causes a premature stop of bundle
87 sheath cell division, which blocks further tumor expansion.
88

89 Sts2 is secreted and translocated into host nucleus

90 Sts2 encodes a small protein containing 183 amino acids (aa), including a 27 aa N-terminal
91 signal peptide (SP). To test for secretion, we expressed Sts2-mcherry in the CR-Sts2 mutant
92 under control of the *pit2* promoter, which confers a high expression level throughout plant
93 infection **(Fig. 2a)**[25]**.** In confocal microscopy, Sts2-mcherry accumulated on the edge of
94 biotrophic hyphae (similar to the effector control Pit2-mcherry[25]) indicating secretion during
95 maize infection. **(Fig. 2a, b).** In contrast, the mcherry alone was localized in the cytoplasm of
96 hyphae cell **(Fig. 2c)**. Next, we determined the subcellular localization of Sts2 in the plant by
97 transient expression of Sts2$^{\Delta SP}$-GFP in *Nicotiana benthamiana* **(Fig. 2d)**. The specific nuclear
98 localization of Sts2$^{\Delta SP}$ suggests that Sts2 might be translocated into the host cells upon secretion
99 by *U. maydis* **(Fig. 2d)**. To test this, we complemented the *U. maydis* CR-Sts2 mutant with a

100 Pro^{Sts2}::Sts2-3×HA construct. The expression of the Sts2-3xHA fusion protein fully restored
101 virulence, indicating that the C-terminal HA-tags did not affect the virulence function of Sts2
102 **(Fig. 3g)**. 4 dpi leaves from Pro^{Sts2}::Sts2-3×HA infection were collected and followed up with
103 cell fractionation to detect subcellular localization of Sts2-3×HA **(Fig. 2e)**. By western blot,
104 we could detect Sts2 in the nuclear component, more precisely in the fraction associated with
105 chromatin pellet after nucleoplasm extraction **(Fig. 2e)**. Together, this data shows that Sts2 is
106 a secreted *U. maydis* effector which is translocated into the host nucleus.
107

108 ## Sts2 has *trans* activator function

109 To elucidate the molecular function of Sts2, we attempted to use the yeast two hybrid system
110 to identify potential maize interactors. When we fused Sts2 with Gal4 DNA binding domain
111 (BD), the recombinant protein exhibited a strong activation of reporter genes and grew on
112 dropout plate **(Fig. 3a)**, which implied that Sts2 may have a transactivation function. Using the
113 9aaTAD tool (https://www.med.muni.cz/9aaTAD/), we identified two overlapping nine aa
114 (DTATANAAL and ATANAALQP) transactivation domains (TAD) in Sts2 **(Fig. 3b)**. To test
115 the function of the predicted TAD, we mutated the domain ATANAALQP, since it was
116 identified by "less stringent" and "pattern for clusters" models. We generated two different
117 mutants by changing ATANAALQP into the corresponding aligned amino acids
118 (EQAREHIQA) of the orthologous protein Sr10075 (Srad) from *S. reilianum*, or deleting the
119 entire motif (dTAD). To minimize the noise expression of the reported genes in yeast, we
120 adapted the positive interaction control p53 and T antigen used in yeast two hybrid assay by
121 fusing Sts2 with T antigen to replace the Gla4 activation domain **(Fig. 3c)**. The interaction
122 between p53 and antigen T brings Sts2 to the proximal of the promoter upstream the reporter
123 genes thus activating their expression **(Fig. 3d)**. As expected, co-transformation of BD-p35
124 with T-$Sts2^{\Delta SP}$_Srad or T-$Sts2^{\Delta SP}$_dTAD failed to grow on dropout plate, indicating the loss of
125 transactivation activity in the mutant proteins **(Fig. 3d)**. In a next step, we tested the *trans*
126 activation of Sts2 *in planta*. To this end, we set-up an effector-GFP reporter system in
127 *Nicotiana benthamiana* **(Fig. 3e)**. In consistency with the yeast experiments, DB-$Sts2^{\Delta SP}$
128 significantly induced GFP expression in *N. benthamiana* driven by the $Pro^{5\times UAS\text{-}35Smini}$ **(Fig. 3f).**
129 This induction was significantly reduced or completely abolished, when the TAD was mutated
130 or deleted, respectively **(Fig. 3g)**. Thus, Sts2 is a transcriptional activator *in-planta*, and this
131 activity depends on its TAD motif. A crucial question is, if this activity is necessary for the
132 virulence function of Sts2. To test this, we genetically complemented *U. maydis* CR-Sts2 with

133 either, wild-type Sts2, Sts2_Srad or Sts2_dTAD mutant under its native promoter and used the
134 resulting strains for plant infection assays. While wild-type Sts2 complementation completely
135 restored virulence, strains expressing TAD-mutated versions showed reduced tumor formation
136 similar to the CR-Sts2 **(Fig. 3h)**. This suggests that the *trans* activation function of Sts2,
137 mediated by the TAD, is crucial for its virulence function.
138

139 Sts2 interacts with ZmNECAP1, a putative maize transcriptional activator

140 Sts2 does neither contain canonical DNA binding domains, nor nuclear localization signals,
141 which suggests that it is a transcriptional activator, and participates in the hosts gene regulation
142 network. To understand how Sts2 activates host gene expression, we performed a co-
143 immunoprecipitation (co-IP) to identify the interacting host proteins. For this, CR-Sts2
144 expressing the Sts2-3×HA was infected to maize leaves for subsequent sample preparation. As
145 a control, *U. maydis* SG200 expressing GFP-3×HA (with the N-terminal secretion signal of
146 Sts2, and expressed under control of the native sts2 promoter) was used. The
147 immunoprecipitated proteins were subjected to mass spectrometry for protein identification. In
148 total, 7 maize proteins were exclusively detected in Sts2-3×HA samples but not in the GFP-
149 3×HA controls from at least 3 independent biological replicates **(Supplementary Table 1)**. Of
150 these, we could independently confirm the interaction of Sts2 with Zm00001eb221890 both by
151 co-IP **(Fig. 4a)** and split luciferase complementation assay in *N. benthamiana* **(Fig. 4b)**.
152 Zm00001eb221890, which is predicted as an adaptin-ear-binding coat-associated protein 1
153 (ZmNECAP1 hereafter) containing a pleckstrin homology domain, shows expression in maize
154 leaves, and displays significant transcriptional induction upon *U. maydis* infection
155 **(Supplementary Fig. 2a).** Subcellular localization identifies ZmNECAP1 in the cytoplasm,
156 nuclear membrane, and it co-localizes with Sts2 in the plant nucleus **(Fig. 4c, Supplementary**
157 **Fig. 2b)**.
158 To our surprise, ZmNECAP1 contains two separated TADs **(Supplementary Fig. 2c)**. Similar
159 to Sts2, a DB-ZmNECAP1 activated the reporter GFP expression under $Pro^{5\times UAS\text{-}35Smini}$ in *N.*
160 *benthamiana* **(Fig. 4d, f),** while deletion of the TADs completely abolished this activity **(Fig.**
161 **4d, f)**. Thus, not only Sts2, but also its maize interactor ZmNECAP1 is a transcriptional
162 activator.
163
164
165

Sts2 activates maize leaf developmental regulators for tumor formation

To determine the host genes potentially regulated by Sts2, we conducted RNA-sequencing. For this purpose, *U. maydis* SG200, CR-Sts2 infected and mock-treated leaves from 3 and 6 dpi were sampled and analyzed. The infection of *U. maydis* dramatically altered maize leaf transcriptome. More than 45.2% of genes (11394 and 13593 genes at 3 and 6 dpi, respectively) were differentially expressed between mock treated and SG200 infected samples **(Supplementary Figure. 3a)**. In general, CR-Sts2 triggered a similar maize transcriptional change at different timepoints to that by SG200 **(Supplementary Figure. 3a)**, which confirms that mutation of Sts2 did neither affect the biotrophic growth of the mutant, nor trigger increased maize immune responses. In total, 5035 genes and 2370 genes were up-regulated or down-regulated, respectively, during the *U. maydis* infection, regardless of the genotype and time point **(Supplementary Figure. 3a, b)**. Gene ontology (GO) enrichment analysis identified genes involved in several cell cycles related biological processes were both up-regulated by SG200 and CR-Sts2 infection **(Supplemental Table 2)**, which is in line with that the *de novo* cell division of bundle sheath were initiated, but prematurely stopped by knockout as shown by transverse section microscopic photo.

To further elucidate key factors that control the sustained hyperplasia cell division, we compared the maize DEG between SG200 and CR-Sts2 infection samples in pairwise. In total, 435 and 465 genes were significantly up-regulated in SG200 samples at 3 and 6 dpi respectively, compared to 271 and 339 genes in CR-Sts2 samples **(Fig. 5a, b)**. GO enrichment analysis revealed that at 3 dpi, genes involved in the "stem cell population maintenance" and "meristem maintenance" are specifically activated by *U. maydis* infection in presence of Sts2 **(Fig. 5c)**. At 6 dpi, in addition to "meristem maintenance", several developmental processes were up-regulated depending on Sts2 **(Fig. 5c)**. Interestingly, from the 83 genes that were consistently, significantly up-regulated in SG200 infected samples at both time points **(Fig. 5b)**, we identified the expression level of several transcription factors and activators were intensified in the presence of Sts2, including *ZmGRF3* (growth-regulating factor 3), *ZmGIF1* (growth-regulating-factor-interacting factor 1), *ZmYAB1* (YABBY1), *ZmSHR1* (short root 1), *ZmWOX5b* (WUSCHEL-Homeobox-transcription factor 5b) and *ZmANT1* (AINTEGUMENTA 1) **(Fig. 5d).** These genes are highly expressed in the dividing zone during leaf development[26] and in maize embryonic leaf cells[27,28]. ZmGRF interacts with ZmGIF, together to determine the shoot meristem in maize[29–31], where ZmANT1, ZmSHR1 and ZmYAB1 are regulators of Kranz anatomy development[27,28,32] and WOX members are well

199 known highly expressing in embryo like cells[33]. Overexpression of some of these genes alone
200 can lead to excess cell division in Arabidopsis[34] , rice[35] and Medicago[36]. While these genes are
201 highly induced upon SG200 infection compared to mock samples, knock out of Sts2 resulted
202 in a strongly reduced expression **(Supplementary. 4)**. Furthermore, CR-Sts2 strains
203 complemented with mutated TAD (Srad and dTAD) also failed to activate the expression of
204 these genes to the levels observed for SG200. Similarly, *U. maydis* strains where UmSts2 was
205 replaced by the open reading frames of the two *S. reilianum* Sts2 orthologs (KI_sr10075 and
206 KI_sr10079) could not induce these maize genes during infection. **(Fig. 5e)**. Together, this
207 shows that the activation of these maize genes requires Sts2 with its functional transactivation
208 motif.

209 To test, if the reduced expression of these genes is specific to Sts2 regulation rather
210 than being a consequence of compromised tumor formation, we checked the expression of
211 these Sts2-induced genes in other *U. maydis* effector mutants being compromised in
212 tumorigenesis. Infection of maize inbred line CML322 with an *U. maydis* deletion mutant for
213 the effector gene *UMAG_02297* resulted in reduced tumors[37]. Re-analysis of corresponding
214 RNA-seq data reveals that *ZmGIF1*, *ZmGRF3, ZmYAB1, ZmSHR1*, and *ZmANT1* were not
215 significantly changed in the *UMAG_02297* knockout compared to SG200, although expression
216 of *ZmWOX5b* could not be detected **(Supplementary Fig. 5a)**. More importantly, qPCR
217 showed that induction of the Sts2-induced maize genes is not affected upon *U. maydis* ΔSee1
218 mutant infection (**Supplementary. 5b**), which displays a similar arrested hyperplasia tumor
219 division phenotype to CR-Sts2[13,20]. All together, these findings confirm a specific induction of
220 the identified maize genes by Sts2.

221 Following our conclusion that Sts2 induces the expression of maize genes required for
222 tumorigenesis, we hypothesized that the transcriptional repression of Sts2-regulated maize
223 genes would result in an inhibition of tumor formation. However, as the maize mutants of these
224 genes are not available, we decided for the alternative approach to fuse a transcriptional
225 suppressor SRDX motif with Sts2. The SRDX motif was shown to turn transcriptional
226 activators into suppressors and moreover, it could inhibit the *trans* activation of its interacting
227 transcription factors /activators[38,39]. Thus, an Sts2-SRDX fusion is expected to act as a
228 dominant suppressive effector. Indeed, in the effector-GFP reporter system, DB-ZmNECAP1
229 activated the expression of GFP under the control of $Pro^{5\times UAS\text{-}35Smini}$::GFP as shown above **(Fig.**
230 **4d,e)**. However, upon co-infiltration with $Sts2^{\Delta SP}$-SRDX, this activation was suppressed by the
231 interaction between ZmNECP1 and $Sts2^{\Delta SP}$-SRDX as expected, but not by the Sts2 fused with

232 mutated SRDX motif (SRDXm) **(Fig. 5f)**. To test the effect of Sts2-SRDX mediated repression
233 in the actual *U. maydis* - maize interaction, we generated *U. maydis* strains over-expressing
234 Sts2-SRDX (or Sts2-SRDXm) to outcompete the native Sts2 and infected them to maize
235 seedlings to evaluate the tumor formation. At 12 dpi, *U. maydis* strains expressing Sts2-SRDX,
236 but not Sts2-SRDXm, showed significantly reduced the tumor formation. This reduction
237 seemed to be dose dependent, as multiple integration of the Sts2-SRDX overexpression
238 construct had an additive effect, resulting in further decreased tumor formation **(Fig. 5g)**. qPCR
239 showed that the transcript levels of Sts2-dependent leaf developmental regulators were
240 significantly inhibited by Sts2-SRDX. Contrary, Sts2-SRDXm did not significantly affect
241 expression of the maize genes, independent of its copy number **(Fig. 5h)**. Notably,
242 overexpression of Sts2-SRDX or Sts2-SRDXm did not completely suppress or further increase
243 the expression of these genes **(Fig. 5h).**
244 We found previously that Sts2 contributes to fungal virulence during leaf infection, but
245 not on tassel, where *U. maydis*-induced tumor formation results from redirecting the intrinsic
246 cell proliferation without an oncogenic activity, as it is seen in leaf tumors [13,24]. In line with
247 this, tassel infection of the Sts2-SRDX and Sts2-SRDXm mutants showed no reduction in
248 virulence compared to strain SG200 **(Fig. 5i).** This underpins that the restricted tumor
249 formation caused by Sts2-SRDX is not consequence of a general inhibition of *U. maydis*
250 virulence, but results from the suppression of tissue specific host developmental regulators.
251 Taken together, we conclude that the Sts2 effector is translocated from fungal hyphae to plant
252 nuclei, where it contributes to tumor formation by activating the expression of leaf
253 development regulators.
254

255 # Discussion

256 *U. maydis* induced tumor formation is a complex and still poorly understood process.
257 During this process, *U. maydis* secretes a group of the tumorigenic effectors which not only
258 prime highly differentiated bundle sheath cells for *de novo* cell division, but also sustains such
259 division to increase the tumor size. Until now, See1 is the only effector which has been shown
260 to re-activate the DNA synthesis, a prerequisite of cell division[20]. Surprisingly, *S. reilianum*
261 SrSee1 protein resembles this function in *U. maydis,* but not UhSee1 from the barley smut
262 fungi *Ustilago hordei*[20,40]. Here, we disclose Sts2 as a tumorigenic effector and, to our best
263 knowledge, the first functionally validated fungal effector which acts as a transcriptional
264 activator in the host. Moreover, we found that the virulence function of Sts2 depends on its

265 transcriptional activation function. Compared to TALE effectors of the bacterial pathogen
266 *Xanthomonas sp*[3], Sts2 lacks a repetitive DNA binding domain, which may be related to the
267 generally small size of fungal effectors to facilitate the secretion into host cell via conventional
268 secretory pathway. The lack of a DNA binding domain also implies that Sts2 needs to recruit
269 host components to form a transcriptional complex to activate target gene expression. We
270 found that Sts2 interacts with ZmNECAP1, a functionally uncharacterized plant transcriptional
271 activator. Here, future investigations on the function of ZmNECAP1 during *U. maydis*-induced
272 tumor formation and leaf development will aim to elucidate whether it is a co-activator with
273 Sts2, or rather a scaffold required by Sts2 to target a DNA binding protein are needed.
274 *U. maydis* infection comprehensively reprograms the leaf developmental process to form
275 tumors, which makes it hard to pinpoint the key host factors related to tumorigenesis. In this
276 study, we show that Sts2 amplifies the expression of a group of plant transcription factors and
277 activators regulating leaf development, after the developed bundle sheath cells are primed for
278 division. We hypothesize that the Sts2-regulated genes are the potential executors to maintain
279 hyperplasia tumor propagation. Accordingly, Sts2-SRDX specifically suppresses these genes,
280 leading to compromised tumor formation on maize leaves, but not on tassel. It will be intriguing
281 to know whether these genes are directly regulated by Sts2, or whether their regulations are
282 decided downstream of Sts2 by yet unknown transcription factors. The results presented in this
283 study demonstrate the potential of microbial effectors as molecular tools to help us explore
284 complex cellular processes in host organisms, such as the network of co-regulation of leaf
285 development regulators. Above all, we continue to be fascinated by the power of evolution to
286 produce the molecular diversity of pathogen-host interactions necessary to adjust highly
287 complex processes such as tumor formation in a cell type-specific manner.
288

289 # Materials and Methods

290 ## Strains and plant material, growth conditions

291 All mutants were generated in *U. maydis* solopathogenic strain SG200 in this study. The *U.*
292 *maydis* strains were grown on PD-agar plate at 28°C or YEPS light liquid medium at 28°C,
293 200 rpm. The maize cultivar Golden Bantam was used for infection (otherwise indicated). The
294 plants were grown at controlled greenhouse or phytochamber with 16 hr light at 28°C and 8 hr
295 dark at 22°C. The CRISPR mutagenesis of Sts2 was done as previous described[23] by the oligo
296 listed in **Supplementary Table 3**. The resulting strains were sent for sequencing to confirm
297 the open reading frame shift and premature stop. For Sts2-SRDX or SRDXm, the amino acid

298 sequence of SRDX (LDLDLELRLGFA) [39] and SRDXm (FDPDQEARFGFA)[38] were first
299 codon optimized in Eurofin online tool, and then assembled with Sts2 open reading frame and
300 Pit2 promoter by Gibson assembly. The constructs were then introduced in SG200 by *ip*
301 integration and further analyzed by southern blot and qPCR to check the integration and copy
302 number (data not shown). The complementary of all CR-Sts2 with Sts2 and Sts2 mutants were
303 done in a similar method.
304
305 **Transactivation activity test.**
306 For the autoactivation test in yeast, the yeast strain AH109 was used. The $StSts2_{28-183}$ was
307 amplified and cloned into pGBKT7 to fuse with Gal4 BD domain, or into pGADT7-T to
308 replace Gal4 AD domain and in open reading frame with antigen T protein. The resulting
309 plasmids were transformed into AH109 alone or with pGBKT7-p53, respectively. The
310 transformation and drop assay were done according to the protocol from manufacturer.
311 For the autoactivation test in *Nicotiana Benthamiana*, the $Sts2_{28-183}$, Gal4-BD domain and
312 promoter 5×UAS-35Smini were cloned into MoClo system with BsaI and BpiI domestication[41],
313 and further used for modular cloning of the corresponding. The constructs were transformed
314 into agrobacterium strain GV3101 by electroporation. The resulting agrobacterium was grown
315 overnight until OD_{600} between 1-2, and suspended in infiltration buffer (10 mM $MgCl_2$, 10 mM
316 MES pH5.6, 200 μM acetosyringone) to OD_{600}=3, incubated in dark for 2 hr. Before infiltration,
317 an equal volume of each strain was mixed with p19 strain to final OD=1. Leaves from 3 dai
318 (days after infiltration) were used for GFP detection by ChecmiDoc MP machine (BioRad),
319 and ImageJ Fiji was used for quantification of GFP intensity. The GFP intensity was
320 normalized to the mock infiltration.
321
322 ## Maize infection and disease scoring
323 For seedling infection, seven-days-old Early Golden Bantam (EGB) seedlings or six-days-old
324 Golden Bantam (GB) seedlings were used. The infection and disease scoring were done as
325 previously described[23]. The disease index was used for statistic test, and Tukey multiple
326 comparison test with Bonferroni adjustment was used for significance test. For tassel infection
327 and scoring were done on maze cultivar Gaspe Flint according to Redkar *et. al.*[42]. For
328 significance test, a similar disease index was used as in seedling infection by assigning index
329 9 to tassel growth stunted, >50% large tumor (7), >50% small tumor (5), <50% large tumor (3),
330 <50% small tumor and normal tassel as 0. Then the disease index was used for statistic test,

331 and Tukey multiple comparison test with Bonferroni adjustment was used for significance test.
332 The biological replications were from independent infection experiments.
333

334 Leaf staining, tissue embedding, sectioning and microscope

335 Wheat germ agglutinin-Alexa Fluor 488 (WGA-AF488) and propidium iodide co-staining was
336 done according to previous description. For tissue embedding, around 1.8-cm leaf sections 3
337 cm below the infection sites were collected and embedded according to Alexandra M, 2017[13].
338 Leaf tissues were arranged in Peel-A-Way™ Einbett-Formen mold, and sectioned into 15 µm
339 for microscope. The microscopy of staining tissues and transverse sections were done by using
340 a Nikon Eclipse Ti inverted microscope with the Nikon Instruments NIS-ELEMENTS software.
341 The GFP and mcherry microscopy were done by using a Leica TCS SP8 confocal laser
342 scanning microscope.
343

344 Co-immunoprecipitation and mass spectrometry in maize

345 Inoculums with OD_{600}=3 and 0.1% tween-20 were used to infect EGB. At 3 dpi, 4 cm length
346 of leaf sections 1 cm below the infection site were collected and ground into fine powder with
347 liquid nitrogen. The powders were incubated in extraction buffer (50mM Tris-HCl pH7.5,
348 150mM NaCl, 10% glycerol, 2mM EDTA, 5mM DTT, 1% Triton X-100 and protease inhibitor)
349 for 30 min on ice and centrifuged twice at 16,000 g, 4 °C for 30 min. 10 µl of anti-HA magnetic
350 beads (Pierce) were added into each supernatant and followed by 1 hr incubation at 4 °C with
351 end-to-end rotation. Afterward, the beads were washed three times with extraction buffer and
352 three times with extraction buffer without Triton X-100. In total, four replications from 4
353 independent infections were prepared and to MS analysis.
354 For MS analysis, dry beads were re-dissolved in 25 µL digestion buffer 1 (50 mM Tris, pH 7.5,
355 2M urea, 1mM DTT, 5 ng/µL trypsin) and incubated for 30 min at 30 °C in a Thermomixer
356 with 400 rpm. Next, beads were pelleted and the supernatant was transferred to a fresh tube.
357 Digestion buffer 2 (50 mM Tris, pH 7.5, 2M urea, 5 mM CAA) was added to the beads, after
358 mixing the beads were pelleted, the supernatant was collected and combined with the previous
359 one. The combined supernatants were then incubated o/n at 32 °C in a Thermomixer with 400
360 rpm; samples were protected from light during incubation. The digestion was stopped by
361 adding 1 µL TFA and samples were desalted with C18 Empore disk membranes according to
362 the StageTip protocol[43].

363 Dried peptides were re-dissolved in 2% ACN, 0.1% TFA (10 µL) for analysis and diluted 1:10
364 for measurement. Samples were analyzed using an EASY-nLC 1000 (Thermo Fisher) coupled
365 to a Q Exactive mass spectrometer (Thermo Fisher). Peptides were separated on 16 cm frit-less
366 silica emitters (New Objective, 75 µm inner diameter), packed in-house with reversed-phase
367 ReproSil-Pur C18 AQ 1.9 µm resin (Dr. Maisch). Peptides were loaded on the column and
368 eluted for 115 min using a segmented linear gradient of 5% to 95% solvent B (0 min : 5%B; 0-
369 5 min -> 5%B; 5-65 min -> 20%B; 65-90 min ->35%B; 90-100 min -> 55%; 100-105 min -
370 >95%, 105-115 min ->95%) (solvent A 0% ACN, 0.1% FA; solvent B 80% ACN, 0.1%FA) at
371 a flow rate of 300 nL/min. Mass spectra were acquired in data-dependent acquisition mode
372 with a TOP15 method. MS spectra were acquired in the Orbitrap analyzer with a mass range
373 of 300–1750 m/z at a resolution of 70,000 FWHM and a target value of 3×10^6 ions. Precursors
374 were selected with an isolation window of 1.3 m/z. HCD fragmentation was performed at a
375 normalized collision energy of 25. MS/MS spectra were acquired with a target value of 10^5
376 ions at a resolution of 17,500 FWHM, a maximum injection time (max.) of 55 ms and a fixed
377 first mass of m/z 100. Peptides with a charge of +1, greater than 6, or with unassigned charge
378 state were excluded from fragmentation for MS^2, dynamic exclusion for 30s prevented repeated
379 selection of precursors.
380

381 **Co-immunoprecipitation in *N. benthamiana*, subcellular fractionation,**
382 **western blot and split Luciferase complementary assay**

383 The agroinfiltration and the co-IP was done as described above. Leaf samples from 2 dai were
384 collected and ground to fine powder. The protein was extract by the following buffer (50mM
385 Tris-HCl pH7.5, 150mM NaCl, 10% glycerol, 10mM ETDA, 1 mM DTT, 1 mM PMSF, 1%
386 IGEPAL CA-630 and protease inhibitor). The Myc-Trap magnetic agarose beads (ChromoTek)
387 were used for immunoprecipitation.
388 The subcellular fractionation was done according to the method from Haring M, 2007[44].
389 Afterwards, the resulting nucleus pellet was split into two halves. One half was used for nuclei
390 lysis followed as Chang L, 2018[45] with some modification. The nuclei pellet was suspended in
391 100 µl glycerol buffer (20 mM Tris-HCl, pH 7.9, 50% glycerol, 75 mM NaCl, 0.5 mM EDTA,
392 1 mM DTT, 1 mM PMSF and Roche protease inhibitor cocktail), then 100 µl prechilled nuclei
393 lysis buffer (10 mM HEPES, pH 7.6, 1 mM DTT, 7.5 mM $MgCl_2$, 0.2 mM EDTA, 0.3 M NaCl,
394 1 M Urea, 1% IGEPAL CA-630, 1 mM PMSF, and Roche protease inhibitor cocktail) was
395 added, vortexed and incubated on ice for 5 min. After centrifugation at 4°C with maximum

396 speed, the supernatant was taken as nucleoplasm fraction and the pellet was washed twice with
397 cold PBS buffer containing 1 mM EDTA. The anti-Myc and anti-HA antibody were used for
398 detection by using ChecmiDoc MP machine (BioRad).
399 Different agrobacterium strains were mix with p19 to the final OD_{600}=1, the leaves from
400 *Nicotiana Benthamiana* were shortly rinsed in water, sprayed with 1 mM D-luciferin (Promega)
401 and kept in dark for 10 min before detection by using ChecmiDoc MP machine (BioRad).
402
403 **DNA and RNA preparation and quantitative PCR**
404 For RNA-seq, at least 15 leaves from individual plants were mixed as one sample, for biomass
405 and gene expression quantification, one sample was mixed from at least 5 individual leaves.
406 Each experiment was repeated three times from three independent infections. DNA was
407 prepared by Buffer A (0.1 M Tris- HCl, 0.05 M EDTA, 0.5 M NaCl, 1.5% SDS) and purified by
408 MasterPure Complete DNA and RNA Purification Kit Bulk Reagents (Epicentre, Madison, WI,
409 USA). RNA was prepared by TRizol according to the manufacturer's protocol, followed by
410 DNaseI digestion. The cDNA synthesis was done by using RevertAid First Strand cDNA
411 Synthesis Kit (Thermo Scientific). The qPCR was done by using GoTaq qPCR mix (Promega)
412 and performed on CFX96 Real-Time PCR Detection System (Bio-Rad). $2^{-\Delta Ct}$ (Ct^{UmPpi}-
413 $CT^{ZmGAPDH}$) and $2^{-\Delta Ct}$ (Ct^{GOI}-$CT^{reference}$) was used to determine the relative biomass and gene
414 expression, respectively and Student's *t-test* was used for statistical analysis of significance.
415
416 **MS and RNA-seq data analysis**
417 For MS data analysis, the raw data were processed using MaxQuant software (version 1.6.3.4,
418 http://www.maxquant.org/)[46] with label-free quantification (LFQ) and iBAQ enabled[47].
419 MS/MS spectra were searched by the Andromeda search engine against a combined database
420 containing the sequences from *Z. mays* (Zmays_284_Ensembl-18_2010-01-
421 MaizeSequence.protein_primaryTranscriptOnly.fasta), the bait protein and sequences of 248
422 common contaminant proteins and decoy sequences. Trypsin specificity was required and a
423 maximum of two missed cleavages allowed. Minimal peptide length was set to seven amino
424 acids. Carbamidomethylation of cysteine residues was set as fixed, oxidation of methionine
425 and protein N-terminal acetylation as variable modifications. Peptide-spectrum-matches and
426 proteins were retained if they were below a false discovery rate of 1%. Statistical analysis of
427 the MaxLFQ values was carried out using Perseus (version 1.5.8.5, http://www.maxquant.org/).
428 Quantified proteins were filtered for reverse hits and hits "identified by site" and MaxLFQ
429 values were log2 transformed. After grouping samples by condition only those proteins were

retained for the subsequent analysis that had two valid values in one of the conditions. Two-sample *t*-tests were performed using a permutation-based FDR of 5%. The Perseus output was exported and further processed using Excel.

The RNA-seq was done in Novogene. Reads were filtered using the Trinity software (v2.9.1) option trimmomatic under the standard settings[48] and then mapped to the reference genome using Bowtie 2 (v2.3.5.1) with the first 15 nucleotides on the 5′-end of the reads being trimmed[49]. The reference genome was the genome assembly of *U. maydis*[50] combined with the assembly of *Z. mays* B73 version 5[51]. Reads were counted using the R package Rsubread (v1.34.7)[52]. The edgeR package v.3.26.8 was used for statistical analysis and determine the differential gene expression by using the pairwise comparison generalized linear models (GLMs). Genes with log2 fold change>1 or <-1 and $p<0.05$ were considered as differentially regulated between SG200 and ΔSts2 samples. The differentially regulated genes between treatment were subjected to gene ontology analysis by using PLAZA 5.0 with default setting.

Data availability

All data that support the findings of this study which are not directly available within the paper (and its supplementary information files) will be available from the corresponding authors (GD, WZ) upon reasonable request. RNAseq raw data are publicly accessible in the NCBI Gene Expression Omnibus with accession number GSE225929. The mass spectrometry proteomics data have been deposited to the ProteomeXchange Consortium via the PRIDE[53] partner repository with the dataset identifier PXD040350

Acknowledgements

This project has received funding from the European Research Council (ERC) under the European Union's Horizon 2020 research and innovation programme (grant agreement No 771035), as well as funding by the Deutsche Forschungsgemeinschaft (DFG, German Research Foundation) under Germany´s Excellence Strategy- EXC-2048/1- Project ID: 390686111 and Research Grant DFG-Az: DO 1421/3-3.

Author contributions

WZ and GD designed the research; WZ performed all molecular experiment, virulence assay and RNA-seq data analysis; JRLD mapped the RNA-seq data; SCS and HN conduced MS and MS data analysis. WZ and GD wrote the paper with contributions from other authors.

463 # References:

464 1. Kay, S., Hahn, S., Marois, E., Hause, G. & Bonas, U. A bacterial effector acts as a plant
465 transcription factor and induces a cell size regulator. *Science (1979)* **318**, 648–651
466 (2007).
467 2. Zlobin, N., Lebedeva, M., Monakhova, Y., Ustinova, V. & Taranov, V. An ERF121
468 transcription factor from *Brassica oleracea* is a target for the conserved TAL-effectors
469 from different *Xanthomonas campestris* pv. *campestris* strains. *Mol Plant Pathol* **22**,
470 618–624 (2021).
471 3. Scholze, H. & Boch, J. TAL effectors are remote controls for gene activation. *Curr Opin*
472 *Microbiol* **14**, 47–53 (2011).
473 4. Qi, P. *et al.* A *Ralstonia solanacearum* effector targets TGA transcription factors to
474 subvert salicylic acid signaling. *Plant Cell* **34**, 1666–1683 (2022).
475 5. Harvey, S. *et al. Downy Mildew* effector HaRxL21 interacts with the transcriptional
476 repressor TOPLESS to promote pathogen susceptibility. *PLoS Pathog* **16**, e1008835
477 (2020).
478 6. Bindics, J. *et al.* Many ways to TOPLESS-manipulation of plant auxin signaling by a
479 cluster of fungal effectors. *New Phytologist* **236**, 1455–1470 (2022).
480 7. Navarrete, F. *et al.* TOPLESS promotes plant immunity by repressing auxin signaling
481 and is targeted by the fungal effector Naked1. *Plant Commun* **3**, (2022).
482 8. Darino, M. *et al. Ustilago maydis* effector Jsi1 interacts with Topless corepressor,
483 hijacking plant jasmonate/ethylene signaling. *New Phytologist* **229**, 3393–3407
484 (2021).
485 9. Kim, S. *et al.* Two nuclear effectors of the rice blast fungus modulate host immunity
486 via transcriptional reprogramming. *Nat Commun* **11**, 5845 (2020).
487 10. Qin, J. *et al.* The plant-specific transcription factors CBP60G and SARD1 are targeted
488 by a verticillium secretory protein VDSCP41 to modulate immunity. *Elife* **7**, (2018).
489 11. Lanver, D. *et al. Ustilago maydis* effectors and their impact on virulence. *Nat Rev*
490 *Microbiol* (2017) doi:10.1038/nrmicro.2017.33.
491 12. Zuo, W. *et al.* Molecular Interactions between Smut Fungi and Their Host Plants.
492 *Annual Review of Phytopathology* vol. 57 411–430 Preprint at
493 https://doi.org/10.1146/annurev-phyto-082718-100139 (2019).
494 13. Matei, A. *et al.* How to make a tumour: cell type specific dissection of *Ustilago*
495 *maydis*-induced tumour development in maize leaves. *New Phytologist* **217**, 1681–
496 1695 (2018).
497 14. Misas Villamil, J. C. *et al.* A fungal substrate mimicking molecule suppresses plant
498 immunity via an inter-kingdom conserved motif. *Nat Commun* **10**, (2019).
499 15. Ma, L.-S. *et al.* The *Ustilago maydis* repetitive effector Rsp3 blocks the antifungal
500 activity of mannose-binding maize proteins. *Nat Commun* **9**, 1711 (2018).
501 16. Hemetsberger, C., Herrberger, C., Zechmann, B., Hillmer, M. & Doehlemann, G. The
502 *Ustilago maydis* effector Pep1 suppresses plant immunity by inhibition of host
503 peroxidase activity. *PLoS Pathog* **8**, e1002684 (2012).
504 17. Ökmen, B. *et al.* A conserved enzyme of smut fungi facilitates cell-to-cell extension in
505 the plant bundle sheath. *Nat Commun* **13**, 6003 (2022).
506 18. Djamei, A. *et al.* Metabolic priming by a secreted fungal effector. *Nature* **478**, 395–8
507 (2011).

508 19. Tanaka, S. *et al.* A secreted *Ustilago maydis* effector promotes virulence by targeting
509 anthocyanin biosynthesis in maize. *Elife* **2014**, 1–27 (2014).
510 20. Redkar, A. *et al.* A Secreted Effector Protein of *Ustilago maydis* Guides Maize Leaf
511 Cells to Form Tumors. *Plant Cell* **27**, 1332–51 (2015).
512 21. Villajuana-Bonequi, M. *et al.* Cell type specific transcriptional reprogramming of
513 maize leaves during *Ustilago maydis* induced tumor formation. *Sci Rep* **9**, 1–15
514 (2019).
515 22. Lanver, D. *et al.* The biotrophic development of *Ustilago maydis* studied by RNAseq
516 analysis. *Plant Cell* **30**, tpc.00764.2017 (2018).
517 23. Zuo, W., Depotter, J. R. L., Gupta, D. K., Thines, M. & Doehlemann, G. Cross-species
518 analysis between the maize smut fungi *Ustilago maydis* and *Sporisorium reilianum*
519 highlights the role of transcriptional change of effector orthologs for virulence and
520 disease. *New Phytologist* **232**, 719–733 (2021).
521 24. Schilling, L., Matei, A., Redkar, A., Walbot, V. & Doehlemann, G. Virulence of the
522 maize smut *Ustilago maydis* is shaped by organ-specific effectors. *Mol Plant Pathol*
523 **15**, 780–789 (2014).
524 25. Doehlemann, G., Reissmann, S., Aßmann, D., Fleckenstein, M. & Kahmann, R. Two
525 linked genes encoding a secreted effector and a membrane protein are essential for
526 *Ustilago maydis*-induced tumour formation. *Mol Microbiol* **81**, 751–766 (2011).
527 26. Li, P. *et al.* The developmental dynamics of the maize leaf transcriptome. *Nat Genet*
528 **42**, 1060–1067 (2010).
529 27. Liu, W.-Y. *et al.* Maize ANT1 modulates vascular development, chloroplast
530 development, photosynthesis, and plant growth. *Proceedings of the National*
531 *Academy of Sciences* **117**, 21747–21756 (2020).
532 28. Liu, W.-Y. *et al.* Regulators of early maize leaf development inferred from
533 transcriptomes of laser capture microdissection (LCM)-isolated embryonic leaf cells.
534 *Proc Natl Acad Sci U S A* **119**, e2208795119 (2022).
535 29. Zhang, D. *et al. GRF-interacting factor1* Regulates Shoot Architecture and Meristem
536 Determinacy in Maize. *Plant Cell* **30**, 360–374 (2018).
537 30. Li, M. *et al.* GIF1 controls ear inflorescence architecture and floral development by
538 regulating key genes in hormone biosynthesis and meristem determinacy in maize.
539 *BMC Plant Biol* **22**, 1–15 (2022).
540 31. Nelissen, H. *et al.* Dynamic Changes in ANGUSTIFOLIA3 Complex Composition Reveal
541 a Growth Regulatory Mechanism in the Maize Leaf. *Plant Cell* **27**, 1605–1619 (2015).
542 32. Slewinski, T. L. *et al.* Short-root1 plays a role in the development of vascular tissue
543 and Kranz anatomy in maize leaves. *Mol Plant* **7**, 1388–1392 (2014).
544 33. Nardmann, J., Zimmermann, R., Durantini, D., Kranz, E. & Werr, W. WOX Gene
545 Phylogeny in Poaceae: A Comparative Approach Addressing Leaf and Embryo
546 Development. *Mol Biol Evol* **24**, 2474–2484 (2007).
547 34. Lee, B. H. *et al.* The Arabidopsis *GRF-INTERACTING FACTOR* Gene Family Performs an
548 Overlapping Function in Determining Organ Size as Well as Multiple Developmental
549 Properties. *Plant Physiol* **151**, 655–668 (2009).
550 35. Henry, S. *et al.* SHR overexpression induces the formation of supernumerary cell
551 layers with cortex cell identity in rice. *Dev Biol* **425**, 1–7 (2017).
552 36. Dong, W. *et al.* An SHR – SCR module specifies legume cortical cell fate to enable
553 nodulation. *Nature* (2020) doi:10.1038/s41586-020-3016-z.

37. Schurack, S., Depotter, J. R. L., Gupta, D., Thines, M. & Doehlemann, G. Comparative transcriptome profiling identifies maize line specificity of fungal effectors in the maize– *Ustilago maydis* interaction. *The Plant Journal* **106**, 733–752 (2021).
38. Matsui, K. & Ohme-Takagi, M. Detection of protein-protein interactions in plants using the transrepressive activity of the EAR motif repression domain. *The Plant Journal* **61**, 570–578 (2010).
39. Hiratsu, K., Matsui, K., Koyama, T. & Ohme-Takagi, M. Dominant repression of target genes by chimeric repressors that include the EAR motif, a repression domain, in *Arabidopsis*. *The Plant Journal* **34**, 733–739 (2003).
40. Redkar, A., Villajuana-Bonequi, M. & Doehlemann, G. Conservation of the *Ustilago maydis* effector see1 in related smuts. *Plant Signal Behav* **10**, e1086855 (2015).
41. Weber, E., Engler, C., Gruetzner, R., Werner, S. & Marillonnet, S. A Modular Cloning System for Standardized Assembly of Multigene Constructs. *PLoS One* **6**, 16765 (2011).
42. Redkar, A. & Doehlemann, G. *Ustilago maydis* Virulence Assays in Maize. *Bio Protoc* **6**, (2016).
43. Rappsilber, J., Ishihama, Y. & Mann, M. Stop and Go Extraction Tips for Matrix-Assisted Laser Desorption/Ionization, Nanoelectrospray, and LC/MS Sample Pretreatment in Proteomics. *Anal Chem* **75**, 663–670 (2003).
44. Haring, M. *et al.* Chromatin immunoprecipitation: Optimization, quantitative analysis and data normalization. *Plant Methods* **3**, 1–16 (2007).
45. Liu, C. *et al.* Arabidopsis ARGONAUTE 1 Binds Chromatin to Promote Gene Transcription in Response to Hormones and Stresses. *Dev Cell* **44**, 348-361.e7 (2018).
46. Cox, J. & Mann, M. MaxQuant enables high peptide identification rates, individualized p.p.b.-range mass accuracies and proteome-wide protein quantification. *Nature Biotechnology 2008 26:12* **26**, 1367–1372 (2008).
47. Tyanova, S., Temu, T. & Cox, J. The MaxQuant computational platform for mass spectrometry-based shotgun proteomics. *Nature Protocols 2016 11:12* **11**, 2301–2319 (2016).
48. Grabherr, M. G. *et al.* Full-length transcriptome assembly from RNA-Seq data without a reference genome. *Nature Biotechnology 2011 29:7* **29**, 644–652 (2011).
49. Langmead, B. & Salzberg, S. L. Fast gapped-read alignment with Bowtie 2. *Nature Methods 2012 9:4* **9**, 357–359 (2012).
50. Kämper, J. *et al.* Insights from the genome of the biotrophic fungal plant pathogen *Ustilago maydis*. *Nature 2006 444:7115* **444**, 97–101 (2006).
51. Hufford, M. B. *et al.* De novo assembly, annotation, and comparative analysis of 26 diverse maize genomes. *Science (1979)* **373**, 655–662 (2021).
52. Liao, Y., Smyth, G. K. & Shi, W. The R package Rsubread is easier, faster, cheaper and better for alignment and quantification of RNA sequencing reads. *Nucleic Acids Res* **47**, e47–e47 (2019).
53. Perez-Riverol Y, Bai J, Bandla C, Hewapathirana S, García-Seisdedos D, Kamatchinathan S, Kundu D, Prakash A, Frericks-Zipper A, Eisenacher M, Walzer M, Wang S, Brazma A, Vizcaíno JA. The PRIDE database resources in 2022: A Hub for mass spectrometry-based proteomics evidences. Nucleic Acids Res 50(D1):D543-D552. (2022)

601 # Figure Legends

602

603 **Fig1. Sts2 regulates the hyperplastic tumor cell formation. a,** Image shows the difference
604 of the phenotype between SG200 and CR-Sts2 in maize leaf infections at 12 dpi, representative
605 leaves were photographed. **b,** Microscopic images show the infected maize cells from SG200
606 and CR-Sts2 at 2 dpi. Green indicates hyphae from WGA-AF488 staining, and red is cell wall
607 stained by propidium iodide. Representative images are shown. **c,** qPCR shows the relative
608 biomass between SG200 and mutant. **d,** Transverse leaf sections from 12 dpi illustrate the
609 different tumor cells in SG200 and CR-Sts2 infected leaves between two large lateral veins.
610 The cell wall autofluorescence (DAPI channel) is shown. The red arrows point out the
611 hyperplasia tumor cells at the original bundle sheath position. The green arrows denote the
612 hypertrophy tumor cells. Scale bar = 200 μm.

613

614 **Fig2. Sts2 is secreted and translocated into the host cell nucleus. a-c,** *U. maydis* hyphae
615 expressing Sts2-mcherry **(a)**, Pit2-mcherry **(b)** and **(c)** mcherry at 2 dpi. The plots are the
616 mcherry intensities measured from the solid lines indicated in the photos. Scale bar = 10 μm.
617 **d,** Localization of GFP and Sts2-GFP in *N. benthamiana*. Scale bar = 50 μm. **e,** Western blot
618 detection of Sts2-3×HA in different cell fractions from 3 dpi maize leaves. UDP-Glucose-
619 Pyrophosphorylase (UPase) and histone H3 were used as the markers of cytoplasmic and
620 chromatin-associated fractions, respectively. The positions of molecular weight ladder are
621 shown on the right.

622

623 **Fig3. Sts2 is a transcriptional activator. a,** The image shows the BD-Sts2$^{\Delta SP}$ transformed
624 yeast grown on dropout SD medium plate. **b,** Domain arrangement of Sts2. The vertical line
625 shows the position of overlapping TADs, and the amino acid sequences are shown above. The
626 underlined sequences indicate the domain mutated or deleted in the following experiments. **c,**
627 Diagram explains the co-transformation of BD-p53 and T7- Sts2$^{\Delta SP}$ and the interaction between
628 p53 and T7 antigen brings Sts2$^{\Delta SP}$ to the promoter of reporter genes to activate their expressions.
629 **d,** Image showing the growth of yeasts transformed with corresponding constructs on dropout
630 SD plate. **e,** Diagram showing the construct used for agroinfiltration. **f,** GFP detection in *N.*
631 *benthamiana* leaf co-infiltrated with the corresponding constructs together with Pro$^{5\times UAS-}$
632 ^{35Smini}::GFP. The dashed circles indicate the infiltration area. **g,** Relative GFP intensity from
633 three biological replications. The intensity was normalized to mock. Data shown are the mean

634 value ± SD from 3 biological replication of 3 independent infiltrations. Student's *t-test* was
635 used for significance analysis. **, $p<0.01$. ***, $p<0.001$. **h,** The disease symptoms of SG200,
636 CR-Sts2 and complementation strains with Sts2 and different Sts2 variants. N is the total
637 number of plants infected from 4 independent infections. The letters are the significance levels
638 between different strains. The Tukey Multiple Comparison test with Bonferroni *p* adjusted was
639 performed to determine the significance.
640
641 **Fig4. Sts2 interacts with a novel maize transcription activator ZmNECAP1. a.** Western
642 blot detection of co-immunoprecipitation experiment in *N. benthamiana*. **b.** Split luciferase
643 complementary assay in *N. benthamiana* shows the interaction between $Sts2^{\Delta SP}$ and
644 ZmNECAP1. The circles indicate the infiltration area. **c.** Microscope photos show the co-
645 localization of $Sts2^{\Delta SP}$ and ZmNECAP1 in nucleus. The red is ZmNECAP1-mcherry, and the
646 green is $Sts2^{\Delta SP}$-GFP. The GFP and mcherry intensities were measured from the solid white
647 line as shown in the "Merge". Scale bar = 10 μm. **d.** The image shows the expression of DB-
648 ZmNECAP1 activated $Pro^{5\times UAS\text{-}35Smini}$::GFP. The dashed circles indicate the infiltration area.
649 **e.** The bar plot shows the GFP intensity from three biological replications of three independent
650 infiltrations. Data shown are the mean value ± SD and normalized to the Mock. Student's *t-test*
651 was used to determine the significance. "*", $p<0.05$.
652
653 **Fig5. Sts2 activates regulators of maize leaf development. a,** Bar plot shows number of
654 genes significantly up- or down-regulated in SG200 compared to CR-Sts2 at 3 and 6 dpi. **b,**
655 Venn diagram shows a total of 83 genes were consistently up-regulated upon SG200 infection
656 from both timepoints compared to CR-Sts2. **c,** The dot plot shows GO enrichment analysis of
657 DEGs. **d,** The heatmap shows the expression levels of differentially expressed transcription
658 regulators at both timepoints between SG200 and CR-Sts2 infection. The Z score normalization
659 was performed on the log_2CPM (counts per million) of each gene across samples. **e,** The
660 quantitative RT-PCR results show the expression levels of *ZmGRF3*, *ZmGIF1*, *ZmYAB1*,
661 *ZmSHR1*, *ZmWox5b* and *ZmANT1* upon infection of different strains. Data shown are the mean
662 value ± SD from 3 biological replications of 3 independent infections, the solid points indicate
663 the value of each replication. Student's *t-test* was used for significance test of the expression
664 levels between SG200 and mutants. "*", $p<0.05$, "**", $p<0.01$. **f,** $Sts2^{\Delta SP}$-SRDX suppresses
665 the transactivation function of ZmNECAP1. A level2 MoClo construct containing the $Pro^{5\times UAS\text{-}}$
666 ^{35Smini}::GFP and DB-ZmNECAP1 was co-infiltrated with respective construct shown in the

667 photo. The dashed circles indicate the infiltration area. **g,** The disease scoring of GB infected
668 by SG200, and SG200 overexpressing Sts2-SRDX and Sts2-SRDXm. The experiment was
669 repeated three times with independent infection, n is the total number of infected plants. The
670 letter denotes the significance level between each strain. The Tukey Multiple Comparison test
671 with Bonferroni *p* adjust was performed to determine the significance. **h**, qPCR quantification
672 of the expression levels of leaf developmental regulators upon SG200, SG200 overexpression
673 Sts2-SRDX and Sts2-SRDXm infection at 6 dpi. Data shown are the mean value ± SD from 3
674 biological replications of 3 independent infections, the solid points indicate the value of each
675 replication. Student's *t-test* was used for significance test of the expression levels between
676 SG200 and mutants. "*", $p<0.05$, "**", $p<0.01$.

677

678 # Supplementary Information

679

680 **Supplementary Fig1. Sts2 is induced during *U. maydis* infection and regulates hyperplasia**
681 **tumor formation. a,** The disease symptoms of SG200, CR-Sts2 on maize cultivar Early
682 Golden Bantam. N is the total number of plants infected from 3 independent infections. "*",
683 $p<0.05$. The Student's *t-test* was used for statistic test. **b,** The expression of Sts2 in *U. maydis*
684 FB1×FB2 during the whole biotrophic infection from published data. **c,** More microscope
685 photos of transverse section from SG200 and CR-Sts2 at 12 dpi on maize cultivar Golden
686 Bantam. Each photo represents the typical phenotype from individual plant.

687

688 **Supplementary Fig2. ZmNECAP1 is a plant transcriptional activator induced during *U.***
689 ***maydis* infection. a,** The expression of ZmNECAP1 is induced during *U. maydis* FB1×FB2
690 infection from previously published data. **b,** The subcellular localization of ZmNECAP1 in *N.*
691 *benthamiana.* **c,** The domain arrangement of ZmNECAP1. Two vertical lines indicate the
692 position of the separated two TADs and the amnio acid sequences are shown above.

693

694 **Supplementary Fig3. Differentially expressed maize genes between *U. maydis* SG200 vs**
695 **mock. a,** The Venn diagrams show the numbers of differentially expression genes between
696 SG200vs. Mock and CR-Sts2 vs. Mock at 3 and 6 dpi, respectively. **b,** The intersection
697 diagrams show the gene numbers in different paired comparison.

698

699 **Supplementary Fig4. The expression of maize genes upon *U. maydis* infection in RNA-seq**
700 **samples by qPCR.** The expression level of leaf developmental regulators detected by qPCR
701 in RNA-seq samples. The value of $2^{-\Delta Ct}$ between gene of interest (GOI) and *ZmGAPDH* are
702 calculated and plotted.
703
704 **Supplementary Fig5. The expression of maize genes upon different *U. maydis* effector**
705 **mutants' infection. a,** The relative expression levels of maize leaf developmental regulators
706 upon SG200 and KO_UMAG_02297 infection in maize line CML322 at 3 dpi from published
707 data[37]. The CPM (counts per million) are plotted. **b,** The expression of leaf developmental
708 regulators in SG200 and ΔSee1 mutant infected Golden Bantam at 6dpi by qPCR. The values
709 of $2^{-\Delta Ct}$ between GOI and *ZmGAPDH* are calculated and plotted.
710
711 **Supplementary Table 1. Mass Spectrometry data**
712 **Supplementary Table 2. Gene ontology analysis of up- and down-regulated genes during**
713 ***U. maydis* infection**
714 **Supplementary Table 3. Oligos sequencing used in the study**
715

Figure 1

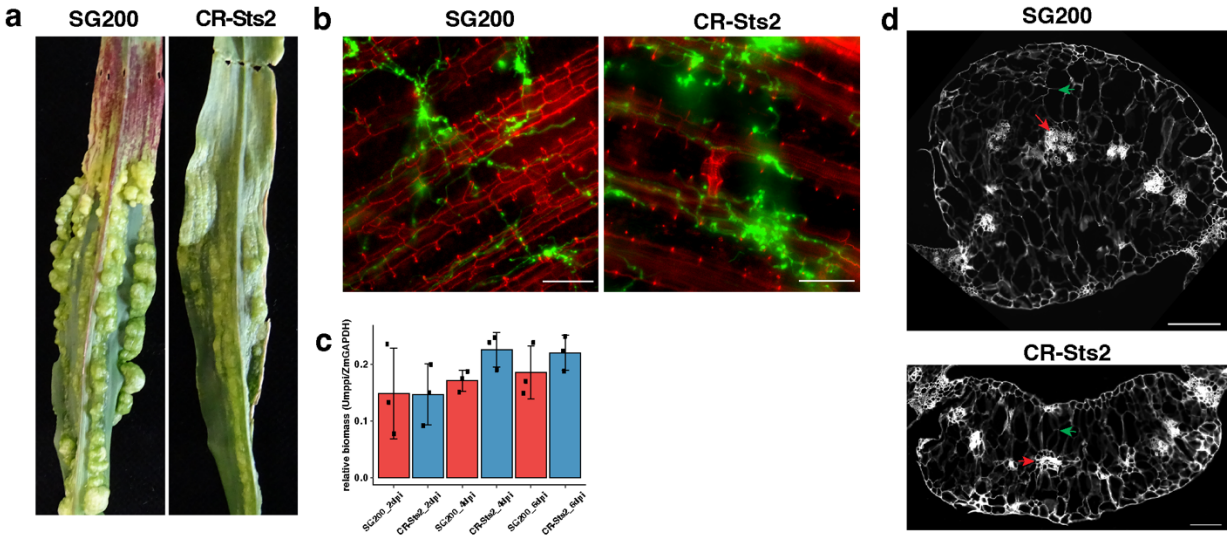

Fig1. Sts2 regulates the hyperplastic tumor cell formation. a, Image shows the difference of the phenotype between SG200 and CR-Sts2 in maize leaf infections at 12 dpi, representative leaves were photographed. **b,** Microscopic images show the infected maize cells from SG200 and CR-Sts2 at 2 dpi. Green indicates hyphae from WGA-AF488 staining, and red is cell wall stained by propidium iodide. Representative images are shown. **c,** qPCR shows the relative biomass between SG200 and mutant. **d,** Transverse leaf sections from 12 dpi illustrate the different tumor cells in SG200 and CR-Sts2 infected leaves between two large lateral veins. The cell wall autofluorescence (DAPI channel) is shown. The red arrows point out the hyperplasia tumor cells at the original bundle sheath position. The green arrows denote the hypertrophy tumor cells. Scale bar = 200 µm.

Figure 2

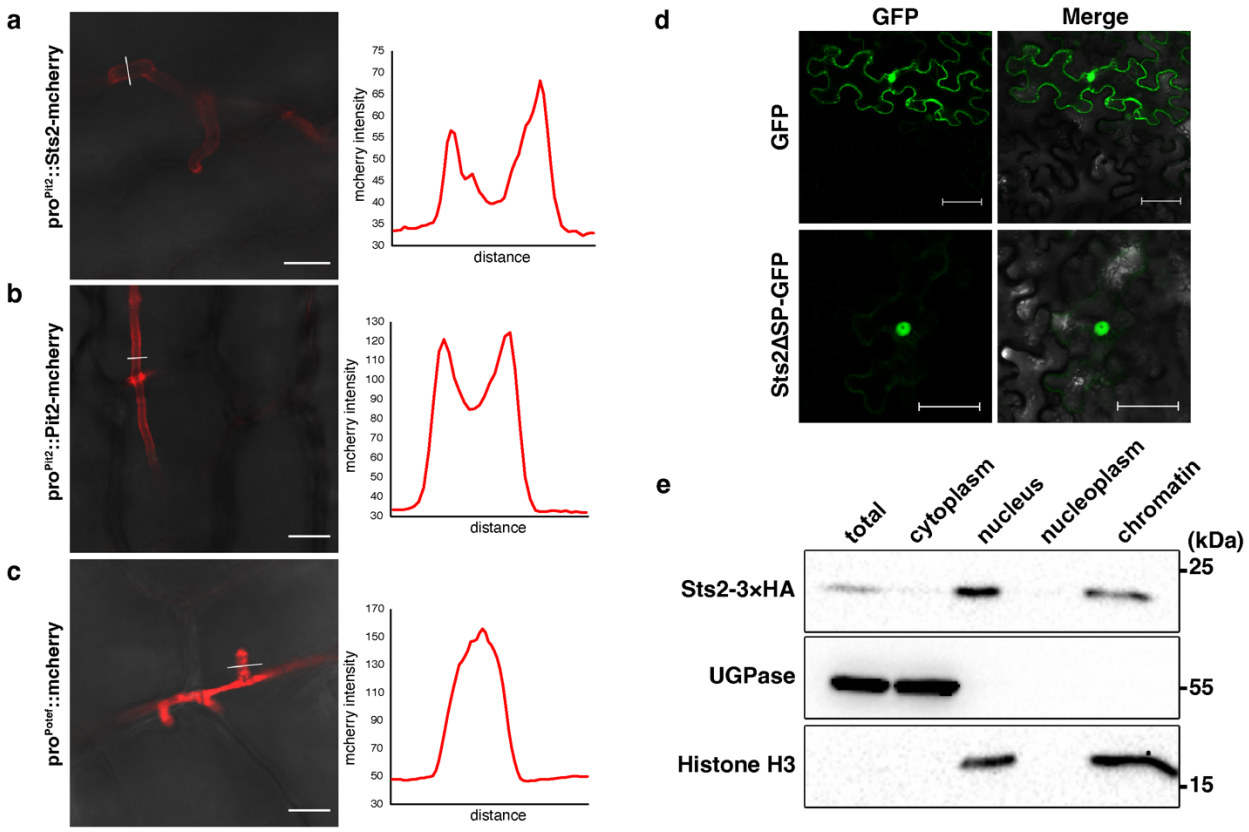

Fig2. Sts2 is secreted and translocated into the host cell nucleus. a-c, *U. maydis* hyphae expressing Sts2-mcherry **(a)**, Pit2-mcherry **(b)** and **(c)** mcherry at 2 dpi. The plots are the mcherry intensities measured from the solid lines indicated in the photos. Scale bar = 10 µm. **d,** Localization of GFP and Sts2-GFP in *N. benthamiana*. Scale bar = 50 µm. **e,** Western blot detection of Sts2-3×HA in different cell fractions from 3 dpi maize leaves. UDP-Glucose-Pyrophosphorylase (UPase) and histone H3 were used as the markers of cytoplasmic and chromatin-associated fractions, respectively. The positions of molecular weight ladder are shown on the right.

Figure 3

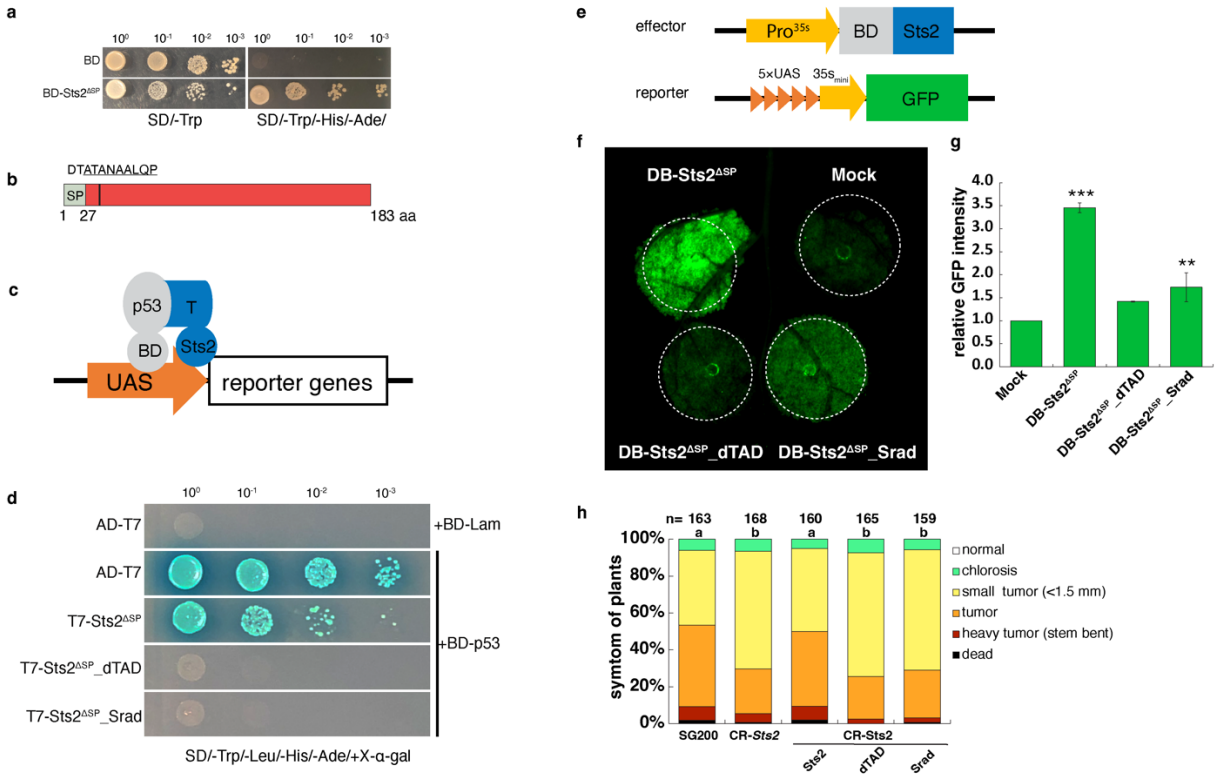

Fig3. Sts2 is a transcriptional activator. a, The image shows the BD-Sts2$^{\Delta SP}$ transformed yeast grown on dropout SD medium plate. **b,** Domain arrangement of Sts2. The vertical line shows the position of overlapping TADs, and the amino acid sequences are shown above. The underlined sequences indicate the domain mutated or deleted in the following experiments. **c,** Diagram explains the co-transformation of BD-p53 and T7- Sts2$^{\Delta SP}$ and the interaction between p53 and T7 antigen brings Sts2$^{\Delta SP}$ to the promoter of reporter genes to activate their expressions. **d,** Image showing the growth of yeasts transformed with corresponding constructs on dropout SD plate. **e,** Diagram showing the construct used for agroinfiltration. **f,** GFP detection in *N. benthamiana* leaf co-infiltrated with the corresponding constructs together with Pro$^{5\times UAS-35Smini}$::GFP. The dashed circles indicate the infiltration area. **g,** Relative GFP intensity from three biological replications. The intensity was normalized to mock. Data shown are the mean value ± SD from 3 biological replication of 3 independent infiltrations. Student's *t-test* was used for significance analysis. **, $p<0.01$. ***, $p<0.001$. **h,** The disease symptoms of SG200, CR-Sts2 and complementation strains with Sts2 and different Sts2 variants. N is the total number of plants infected from 4 independent infections. The letters are the significance levels between different strains. The Tukey Multiple Comparison test with Bonferroni *p* adjusted was performed to determine the significance.

Figure 4

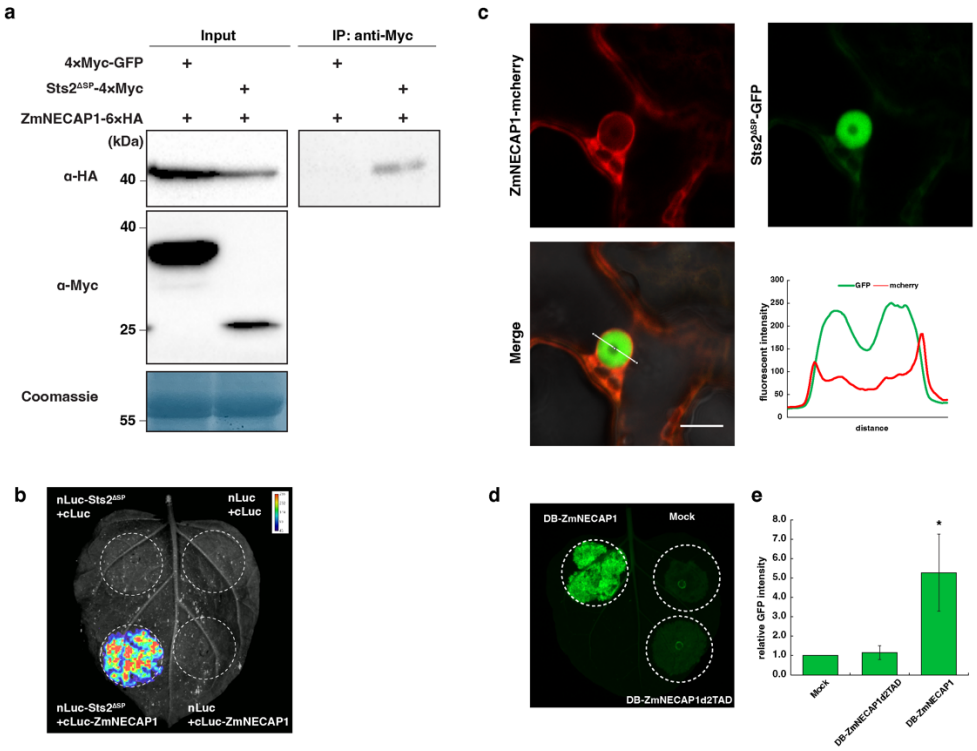

Fig4. Sts2 interacts with a novel maize transcription activator ZmNECAP1. a. Western blot detection of co-immunoprecipitation experiment in *N. benthamiana*. **b.** Split luciferase complementary assay in *N. benthamiana* shows the interaction between Sts2$^{\Delta SP}$ and ZmNECAP1. The circles indicate the infiltration area. **c.** Microscope photos show the co-localization of Sts2$^{\Delta SP}$ and ZmNECAP1 in nucleus. The red is ZmNECAP1-mcherry, and the green is Sts2$^{\Delta SP}$-GFP. The GFP and mcherry intensities were measured from the solid white line as shown in the "Merge". Scale bar = 10 μm. **d.** The image shows the expression of DB-ZmNECAP1 activated Pro$^{5\times UAS\text{-}35Smini}$::GFP. The dashed circles indicate the infiltration area. **e.** The bar plot shows the GFP intensity from three biological replications of three independent infiltrations. Data shown are the mean value ± SD and normalized to the Mock. Student's *t-test* was used to determine the significance. "*", $p<0.05$.

Figure 5

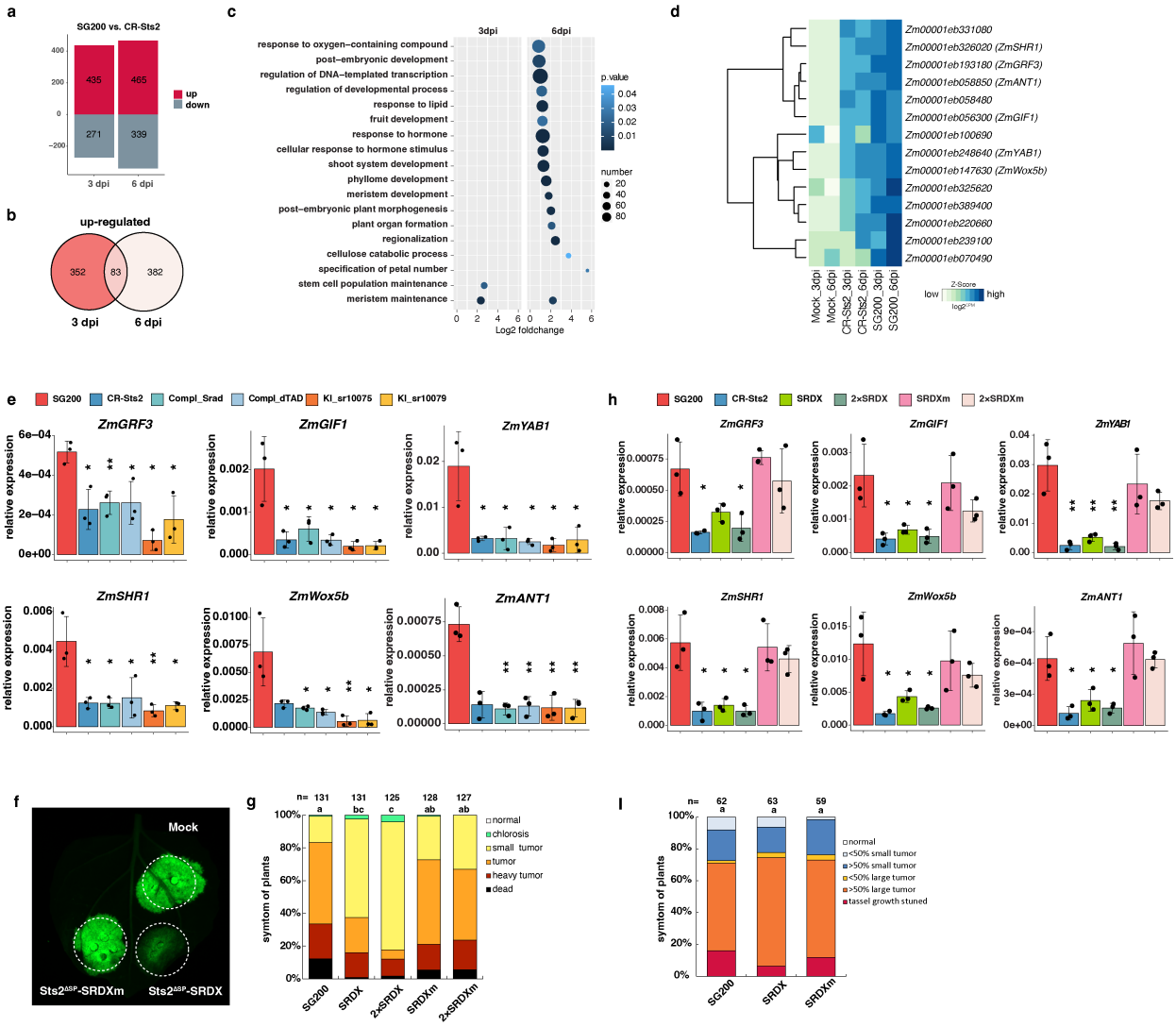

Fig5. Sts2 activates regulators of maize leaf development. a, Bar plot shows number of genes significantly up- or down-regulated in SG200 compared to CR-Sts2 at 3 and 6 dpi. **b,** Venn diagram shows a total of 83 genes were consistently up-regulated upon SG200 infection from both timepoints compared to CR-Sts2. **c,** The dot plot shows GO enrichment analysis of DEGs. **d,** The heatmap shows the expression levels of differentially expressed transcription regulators at both timepoints between SG200 and CR-Sts2 infection. The Z score normalization was performed on the $\log_2$CPM (counts per million) of each gene across samples. **e,** The quantitative RT-PCR results show the expression levels of *ZmGRF3*, *ZmGIF1*, *ZmYAB1*, *ZmSHR1*, *ZmWox5b* and *ZmANT1* upon infection of different strains. Data shown are the mean value ± SD from 3 biological replications of 3 independent infections, the solid points indicate the value of each replication. Student's *t-test* was used for significance test of the expression levels between SG200 and mutants. "*", $p<0.05$, "**", $p<0.01$. **f,** Sts2$^{\Delta SP}$-SRDX suppresses the transactivation function of ZmNECAP1. A level2 MoClo construct containing the Pro$^{5\times UAS\text{-}35Smini}$::GFP and DB-ZmNECAP1 was co-infiltrated with respective construct shown in the photo. The dashed circles indicate the infiltration area. **g,** The disease scoring of GB infected by SG200, and SG200 overexpressing Sts2-SRDX and Sts2-SRDXm. The experiment was repeated three times with independent infection, n is the total number of infected plants. The letter denotes the significance level between each strain. The Tukey Multiple Comparison test

with Bonferroni *p* adjust was performed to determine the significance. **h**, qPCR quantification of the expression levels of leaf developmental regulators upon SG200, SG200 overexpression Sts2-SRDX and Sts2-SRDXm infection at 6 dpi. Data shown are the mean value ± SD from 3 biological replications of 3 independent infections, the solid points indicate the value of each replication. Student's *t-test* was used for significance test of the expression levels between SG200 and mutants. "*", $p<0.05$, "**", $p<0.01$.